Aalborg Universitet

An original transformer and switched-capacitor (T & SC)-based extension for DC-DC boost converter for high-voltage/low-current renewable energy applications

Hardware implementation of a new T & SC boost converter

Padmanaban, Sanjeevikumar; Bhaskar, Mahajan Sagar; Maroti, Pandav Kiran; Blaabjerg, Frede; Fedák, Viliam

Article

An Original Transformer and Switched-Capacitor (T & SC)-Based Extension for DC-DC Boost Converter for High-Voltage/Low-Current Renewable Energy Applications: Hardware Implementation of a New T & SC Boost Converter

Sanjeevikumar Padmanaban [1,*] , Mahajan Sagar Bhaskar [2] , Pandav Kiran Maroti [3], Frede Blaabjerg [4] and Viliam Fedák [5]

[1] Department of Energy Technology, Aalborg University, 6700 Esbjerg, Denmark
[2] Department of Electrical Engineering, Qatar University, P.O. Box 2713 Doha, Qatar; sagar25.mahajan@gmail.com
[3] Department of Electrical and Electronics Engineering, Marathwada Institute of Technology, Aurangabad, Maharashtra 431028, India; kiranpandav88@yahoo.co.in
[4] Centre for Reliable Power Electronics (CORPE), Department of Energy Technology, Aalborg University, 9100 Aalborg, Denmark; fbl@et.aau.dk
[5] Department of Electrical Engineering and Mechatronics, FEI TU of Košice, Letná 9, 04200 Košice, Slovakia; viliam.fedak@tuke.sk
* Correspondence: san@et.aau.dk; Tel.: +45-71-682-084

check for updates

Abstract: In this article a new Transformer and Switched Capacitor-based Boost Converter (T & SC-BC) is proposed for high-voltage/low-current renewable energy applications. The proposed T & SC-BC is an original extension for DC-DC boost converter which is designed by utilizing a transformer and switched capacitor (T & SC). Photovoltaic (PV) energy is a fast emergent segment among the renewable energy systems. The proposed T & SC-BC combines the features of the conventional boost converter and T & SC to achieve a high voltage conversion ratio. A Maximum Power Point Tracking (MPPT) controller is compulsory and necessary in a PV system to extract maximum power. Thus, a photovoltaic MPPT control mechanism also articulated for the proposed T & SC-BC. The voltage conversion ratio (V_o/V_{in}) of proposed converter is $(1 + k)/(1 − D)$ where, k is the turns ratio of the transformer and D is the duty cycle (thus, the converter provides 9.26, 13.88, 50/3 voltage conversion ratios at 78.4 duty cycle with k = 1, 2, 2.6, respectively). The conspicuous features of proposed T & SC-BC are: (i) a high voltage conversion ratio (V_o/V_{in}); (ii) continuous input current (I_{in}); (iii) single switch topology; (iv) single input source; (v) low drain to source voltage (V_{DS}) rating of control switch; (vi) a single inductor and a single untapped transformer are used. Moreover, the proposed T & SC-BC topology was compared with recently addressed DC-DC converters in terms of number of components, cost, voltage conversion ratio, ripples, efficiency and power range. Simulation and experimental results are provided which validate the functionality, design and concept of the proposed approach.

Keywords: DC-DC boost converter; transformer; switched capacitor; maximum power point tracking; renewable energy; high-voltage; low current

1. Introduction

In recent years the importance of using renewable energies has grown significantly due to the fact that the usage of fossil fuels such as oil, coal, and gas results in environmental pollution and serious greenhouse effects which have a huge influence on the world [1,2]. The demands for energy and power converters have been increasing for the last several decades, due to the greater industrialization, rising population and increased living standards of society [3–9]. The International Energy Agency (IEA) has anticipated that the developing nations are raising their energy utilization at a quicker pace than developed ones and will need to nearly the double their present installed generation facility by the year 2020 for fulfill their energy requirements. The total energy consumption of the world from 1980 to 2025 is depicted in Figure 1a [10–12]. The IEA has also details that more than 1.3 billion people in the developing nations are living with insufficient or without any access to electricity because of the unavailability of electric grid in these regions and other constraints [10–12]. Thus, there is a need for new sources of energy that are cheaper and sustainable with less carbon emissions [13,14]. Photovoltaic energy is considered as a reliable, promising and favorable source and it has various advantages such as being pollution free, long life, low maintenance, etc. [15–18]. In Figure 1b the global cumulated PV capacity (in Gigawatts) from 1996 to 2012, and an estimation (E) by 2020 is shown. It is observed that PV is a fast emergent segment among renewable energy systems [19]. To increase the effectiveness and efficiency of power conditioning to tracking Maximum Power Point (MPP) plays an important role in increasing the conversion efficiency. A PV system has non-linear P-V and I-V characteristics and the generated power depends on the environmental conditions such as solar irradiation and temperature [20–22]. The power of a PV system is higher at the knee point of the P-V characteristic curve, as the MPP keeps on changing according to the varying irradiation levels, a MPPT method is used to track the MPP of the system. The PV grid-connected power system in domestic applications is becoming a fast-rising segment in the PV market [23–26]. Unfortunately, the output voltage of the PV arrays or panels is relatively low. Thus, PV series-connected configurations are generally used in order to satisfy the demand and the high bus voltage requirements of the half and full-bridge, multilevel inverters (MLI) needed to transfer energy to electric grid. This type of system suffers from partial shading, reduced PV module efficiency, and mismatched MPPT control [27,28]. Thus boost converters with high voltage conversion ratio and inverters are required to feed energy to the electric grid. In practice DC-DC converters with high efficiency with low input voltage, high input current, high output voltage and high voltage conversion ratio provide a practicable solution for photovoltaic systems to transfer photovoltaic energy to the electric grid via inverters [29,30].
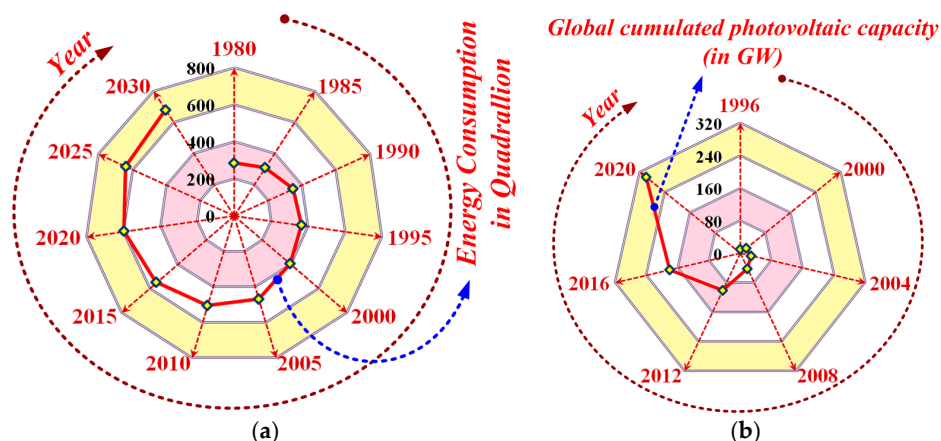

Figure 1. (**a**) Radar plot of energy consumption in quadrillion from 1980 to 2030; (**b**) Radar plot of global cumulated photovoltaic capacity (in GW) from 1996 to 2020.

Additionally, traditional boost converters are not a practicable solution to achieve high conversion ratios due to the leakage resistance of the inductor, high switch stress and the performance of a boost

converter is deteriorated by the high duty cycle of the power switch and thus, not able to achieve conversion ratios of more than four. To operate the DC-DC converters for getting high output voltage without using high duty cycles for power semiconductor controlled switches, isolated converters can be employed which contain transformers, coupled inductors, etc. [29–37], but the usage of such a large number of magnetic components increases the size of the circuit as well as the leakage reactance of the converter and also produces electromagnetic interference which reduces the converter function ability and efficiency. Recently many boost converter topologies are addressed by extending the power circuit of the traditional boost converter. In [38], a single switch *n*-stage Cascaded Boost Converter (*n*-stage CBC) is discussed to achieve high voltage but it requires a large number of inductors, diodes and capacitors. Figure 2a depicts the power circuit of a single switch *n*-stage Cascaded Boost Converter (single switch *n*-stage CBC). In [38], a single switch boost converter with a voltage multiplier extension to achieve high voltage is discussed, but it requires a large number of diodes and capacitor circuitry. Figure 2b depicts the power circuit of a single switch boost converter with voltage multiplier. In [39], a new coupled inductor-based step-up converter is discussed with a large pump. The voltage can be easily achieved by modifying the turns-ratio of coupled inductors but the leakage energy induces high voltage stress and switching losses. The power circuit of coupled inductor based step-up converter is shown in Figure 2c. In [40], a new Quadratic Boost Converter (QBC) with coupled inductor in second boost converter is proposed and shown in Figure 2d. This QBC achieves high step-up voltage gain with an appropriate duty ratio and low voltage stress on the power switch.
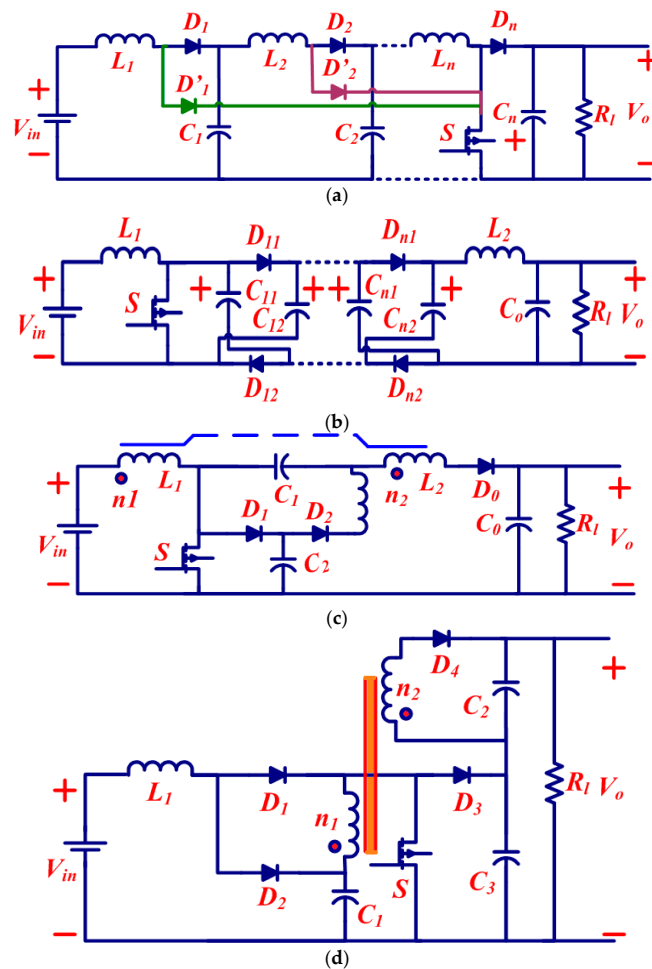

Figure 2. Recently addressed DC-DC power converter circuit (**a**) single switch *n*-stage Cascaded Boost Converter (*n*-stage CBC) (**b**) single switch boost converter with voltage multiplier (**c**) coupled inductor based step-up converter and (**d**) Quadratic Boost Converter (QBC) with coupled inductor.

In [41], a DC-DC non-inverting Nx Interleaved Multilevel Boost Converter (Nx IMBC) is proposed to achieve a high voltage conversion ratio (V_o/V_{in}) and to reduce voltage/current ripple. Nx-IMBC provides N times more voltage conversion ratio compared to traditional boost converters but requires large number of diodes and capacitors. In [42,43], DC-DC non-inverting 2Nx and 4Nx Interleaved Boost converters (2Nx IMBC and 4Nx IMBC) are proposed to achieve high voltage conversion ratio (V_o/V_{in}) and to reduce voltage/current ripple. 2Nx IMBC and 4Nx IMBC provide 2N and 4N times more voltage conversion ratio compared to traditional boost converters, but also require large numbers of diodes and capacitors. To achieve a high inverting voltage conversion ratio, a new inverting Nx and 2Nx Multilevel Boost Converter (MBC) was proposed for renewable energy applications [44]. In [45,46], a new family of DC-DC converters called "X-Y Converter Family" was proposed to achieve high conversion ratios for renewable applications. These converters are well suited to achieve high voltage, but need more number of devices, thus increasing the size and cost of the converter.

In this article, a new T & SC-BC is proposed for high-voltage/low-current renewable applications to overcome the drawback of recently addressed converters. The power circuit and block diagram of proposed converter scheme system is shown in Figure 3. The proposed T & SC-BC is an original extension for DC-DC boost converters which is based on T & SC. The proposed T & SC-BC converter combines the features of a conventional boost converter and T & SC [47] to achieve high voltage conversion ratios. In a PV cell model the current source is basically associated in parallel with the reversed diode and also has series and parallel resistance as shown in Figure 3. Resistance in series (R_S) is due to barrier in the pathway of flow of electrons from *n* to *p* junction and resistance in shunt (R_{Sh}) is due to the leakage current [48]. The relation between the currents of a PV cell is shown in Equation (1):

$$\left. \begin{array}{c} I = I_{ph} - I_d - I_{Sh}, I_d = I_o(e^{\frac{V+IR_S}{nV_T}} - 1), I_{Sh} = \frac{V+IR_S}{R_{Sh}} \\ V_T = \frac{kT}{q}, V_T = 0.0259V \ at \ T = 25\,^\circ\text{C} \end{array} \right\} \tag{1}$$

where I_{ph} is the photocurrent generated by the cell, I_d is the current flowing through the diode of the solar cell, I_{Sh} is the shunt current flowing through the shunt resistance (R_{Sh}), I is the output current or current flowing through the series resistance (R_S), V is the voltage at the output terminal of the cell, I_o is the reverse saturation current, *n* is the diode ideal factor, V_T is the thermal voltage, *k* is the Boltzmann constant and *T* is the absolute temperature. When irradiance strikes the flat surface of a PV module or cell, an electrical field is produced within the cell. In the presence of an electric field, these charges can create a current that can be used in a peripheral circuit. This current depends on the concentration and intensity of the incident solar radiation. The higher the level of the light intensity, the more electrons can be allowed to run free from the flat surface, and the more current is created. All the time it is necessary to track MPP due to deviation of hotness and irradiation of the array [49,50]. MPPT techniques to track MPP have been addressed and published over years of research [50–53]. Every MPPT method has its own merits and demerits like required sensors, complexity, cost, range of effectiveness, convergence speed, correct tracking when the irradiation and temperature change. The Perturb & Observe (P & O) algorithm and Incremental Conductance algorithm is the most popular and simple methods to track MPP. The P & O algorithm is depends on hill climbing concept hence also called "hill-climbing P & O Method". This is one of most used algorithms due to its simplicity and ease of implementation and low cost [49,53]. It operates with a cyclic perturbation (increase or decrease) of the array terminal voltage and by comparing the PV power of last perturbation. If the power increases the perturbation goes with the same direction otherwise it will goes with the reverse direction. In this method, the sign of the last perturbation and the sign of the last increment in the power are used to decide what the next perturbation should be [53]. The concept of the P & O MPPT algorithm is shown in Figure 4a–c with the P-V and I-V characteristics. To extract the maximum power, a P & O MPPT control mechanism is used to locate the MPP for the proposed T & SC-BC.
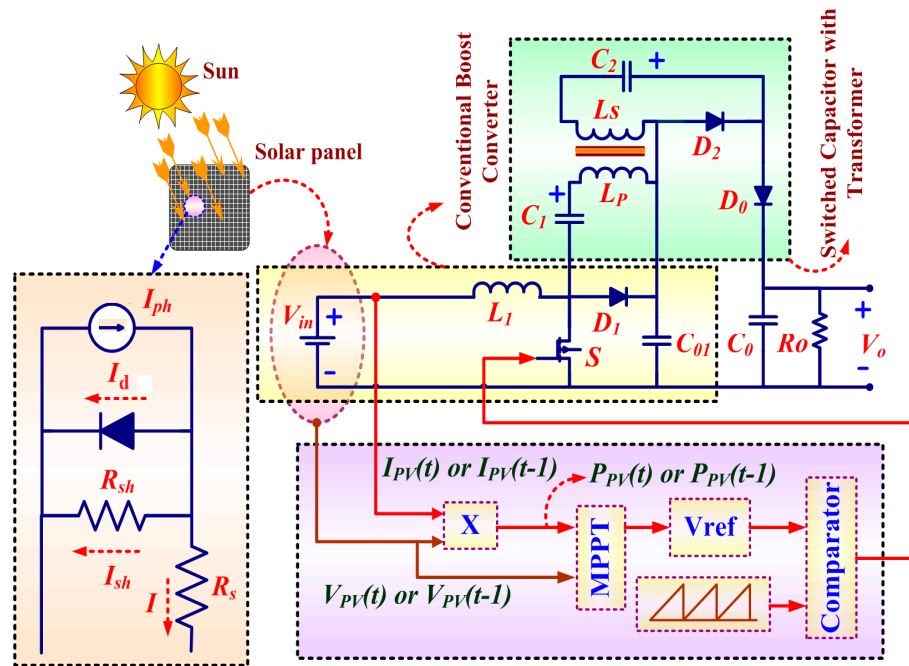
Figure 3. Power circuit and block diagram of proposed converter system: Transformer and Switch Capacitor Based Boost Converter (T & SC-BC) with Maximum Power Point Tracking (MPPT) for high-voltage/low-current renewable applications.
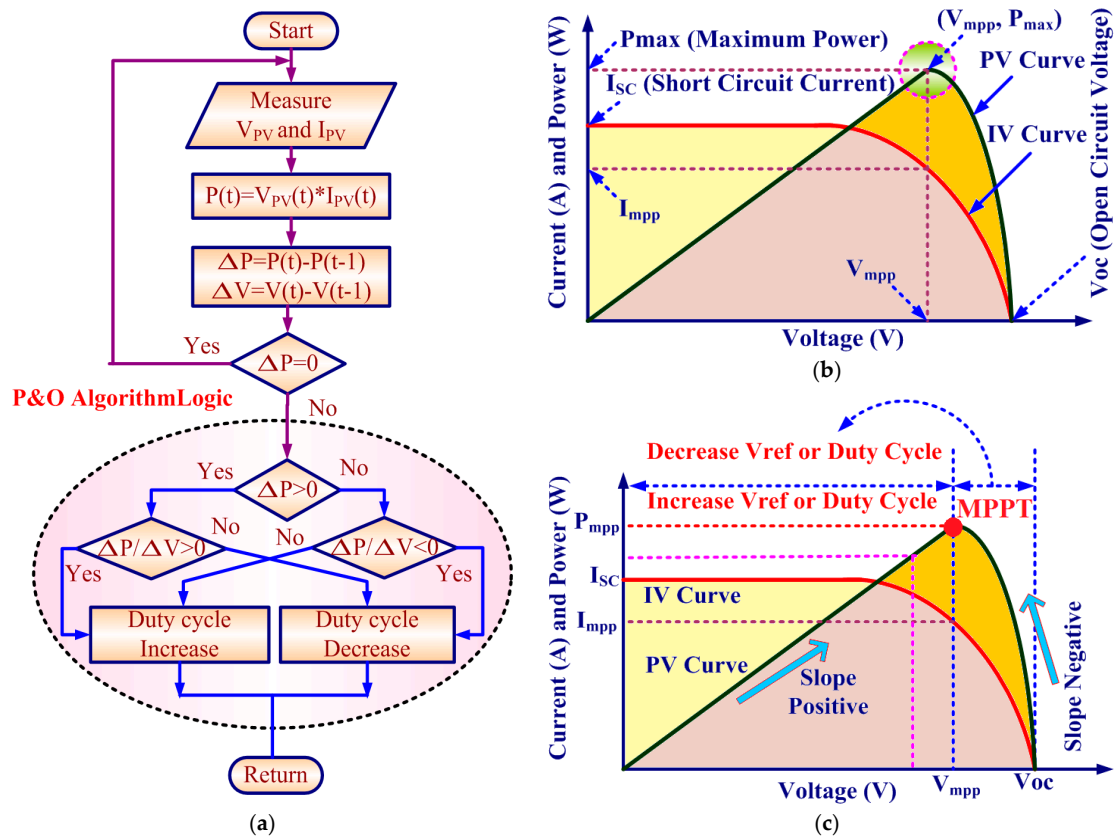
Figure 4. Concept of Maximum Power Point Tracking for proposed T & SC-BC (**a**) Perturb and Observed algorithm (**b**) PV and IV characteristics of photovoltaic cell and (**c**) Concept to track Maximum Power Point (MPP) to extract maximum power.

The conspicuous features of proposed T & SC-BC are:

(1) High voltage conversion ratio (V_o/V_{in}),
(2) Continuous input current (I_{in}),
(3) Single switch topology,
(4) Single input source,
(5) Low Drain to Source voltage (V_{DS}) rating of switch,
(6) Single inductor and single untapped transformer.

Simulation and experimental result are provided which validate the functionality, design and concept of the proposed approach.

## 2. Power Circuit and Operation Modes of Transformer and Switch Capacitor Based Boost Converter (T & SC-BC)

A conventional boost converter with SC or Voltage Doubler (VD) is shown in Figure 5a. A circuit connection of capacitor C_1, C_0 and diode D_2, D_0 forms a SC stage or VD stage. A transformer is employed in the SC stage to provide a T & SC stage for high voltage conversion. The power circuit of the proposed T & SC-BC is shown in Figure 5b. The proposed T & SC-BC is designed by using a conventional/traditional boost converter by employing a T & SC stage at the output side. In Figure 5, inductor L_1, switch S, diode D_1 and capacitor C_{01} form a conventional boost converter. The input supply is directly connected to the conventional boost converter. Capacitor C_1, C_2, diode D_0, D_2 and transformer form the newly designed T & SC stage. L_P is the primary winding of the transformer whose one terminal is connected via capacitor C_1 at the inductor of conventional boost converter or at the drain terminal of a switch and the other terminal is directly connected at the cathode of diode D_1 or at output capacitor C_{01} of the conventional boost converter. L_S is the secondary winding of the transformer whose one terminal is directly connected to the anode of diode D_2 and another terminal connected to capacitor C_2.
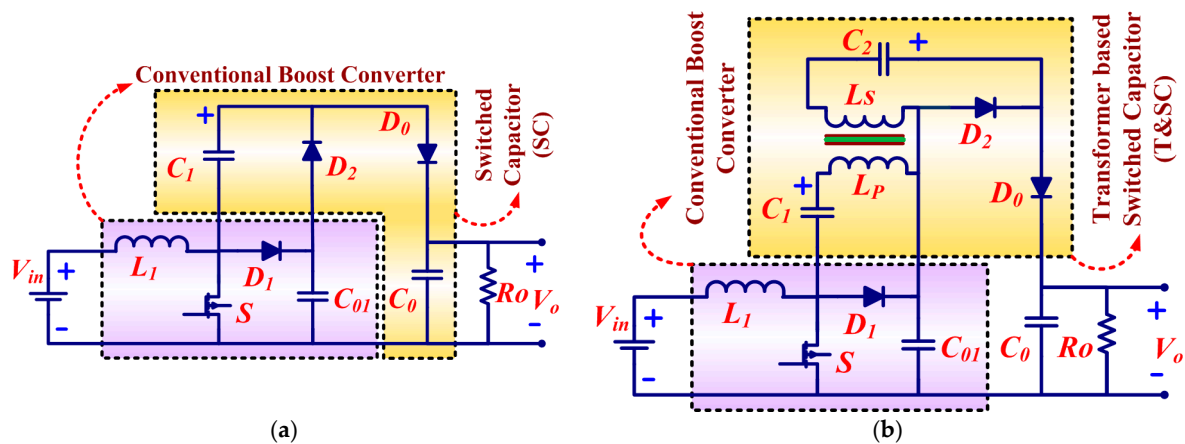
Figure 5. Power circuit of converter (**a**) Conventional boost converter with Switched Capacitor or Voltage Doubler stage and (**b**) Proposed Transformer and Switched Capacitor Based Converter.

The operation of the proposed T & SC-BC is divided into two main modes; one when switch S is turned ON and another when switch S is turned OFF. These two modes are divided into five sub-modes to explain the CCM operation of the proposed T & SC-BC in detail. The CCM characteristic waveforms with the five sub-modes are shown in Figure 6.

Figure 6. Characteristic waveforms of the proposed T & SC-BC in CCM Mode. (Mode-1: time *ta* to *tb*, Mode-2: time *tb* to *tc*, Mode-3: time *tc* to *td*, Mode-4: time *td* to *te* and Mode-5: time *te* to *tf*).

2.1. Mode-1 (Time ta–tb)

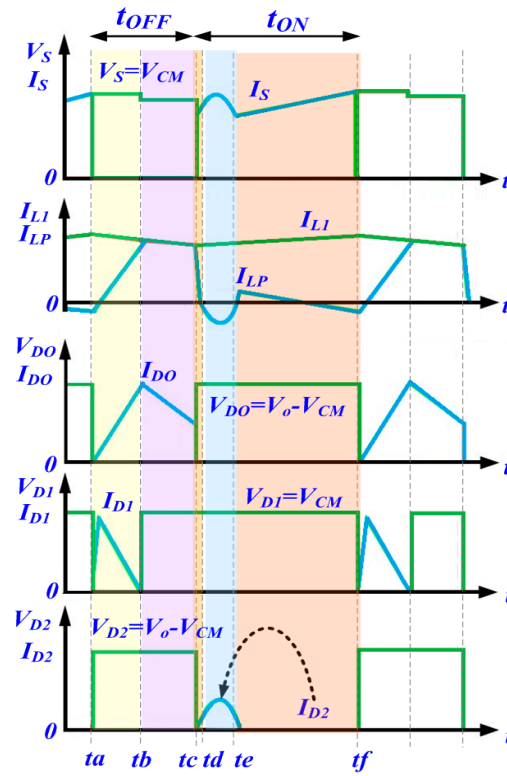In Mode-1, switch S is turned OFF and inductor L_1 is demagnetized. Thus, the energy stored in the inductor L_1 is transferred to capacitor C_{01} through diode D_1. The energy of capacitor C_1, C_2, transformer windings is also transferred through diode D_0 to the output capacitor C_0. The equivalent circuit of the proposed converter for this mode is shown in Figure 7a. In this mode diode D_1, D_0 are operated in forward biased condition whereas diode D_2 are operated in reverse biased condition.

$$\left. \begin{array}{l} Loop-1 \rightarrow V_{in} - V_{L1} - V_{C01} = 0 \\ Loop-2 \rightarrow V_{in} - V_{L1} + VC_1 - V_{LP} - VC_{01} = 0 \\ Loop-3 \rightarrow V_{LS} + VC_2 - V_{CO} + VC_{01} = 0 \end{array} \right\} \tag{2}$$
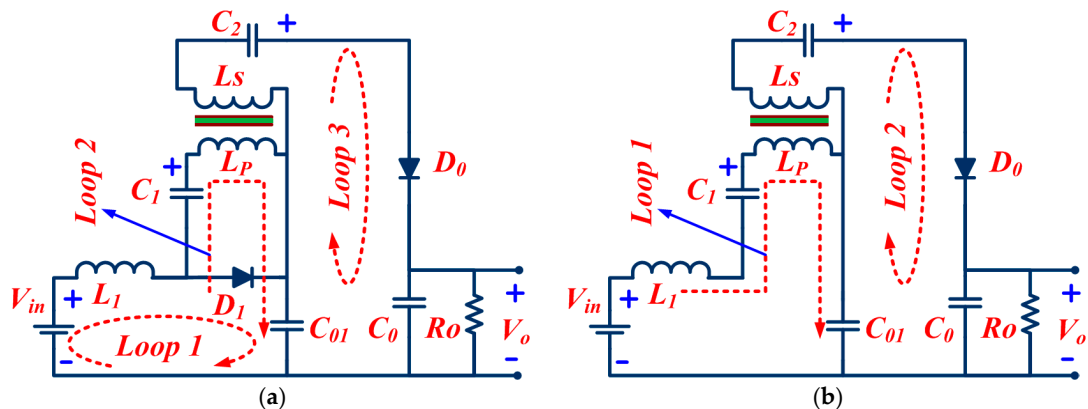

Figure 7. Equivalent circuit of proposed converter when switch S is in OFF state (**a**) Mode-1 (Time *ta–tb*); and (**b**) Mode-2 (Time *tb–tc*).

2.2. Mode-2 (Time tb–tc)

In Mode-2, switch S is turned OFF and inductor L_1 is still demagnetized but the energy stored in the inductor L_1 is not directly transferred to capacitor C_{01} through diode D_1 (diode D_1 is acting as an open circuit) but rather transferred through the windings. The energy of capacitor C_1, C_2, transformer windings is also transferred through diode D_0 to output capacitor C_0. The equivalent circuit of proposed converter for this mode is shown in Figure 7b. In this mode diode D_0 are operated in forward biased condition whereas diode D_1, D_2 are operated in reverse biased condition.

$$\left. \begin{array}{l} Loop-1 \rightarrow V_{in} - V_{L1} + VC_1 = V_{LP} + VC_{01} \\ Loop-2 \rightarrow V_{LS} + VC_2 = V_{CO} - VC_{01} \end{array} \right\} \tag{3}$$

2.3. Mode-3 (Time tc–td)

In Mode-3, switch S is turned ON and inductor L_1 is magnetized through switch S. The energy of capacitor C_1, C_2, transformer windings is transferred through diode D_0 to output capacitor C_0 but the diode D_0 current start decreasing and current slope (di/dt) is limited by the transformer. Hence, the diode reverse current recovery problem is decreased. The equivalent circuit of the proposed converter in this mode is shown in Figure 8a. In this mode diode D_0 are operated in forward biased condition whereas diodes D_1, D_2 are reverse biased.

$$\left. \begin{array}{l} Loop-1 \rightarrow V_{in} - V_{L1} = 0 \\ Loop-2 \rightarrow VC_1 - V_{LP} - VC_{01} = 0 \\ Loop-2 \rightarrow V_{LS} + VC_2 + VC_{01} = V_{CO} \end{array} \right\} \tag{4}$$
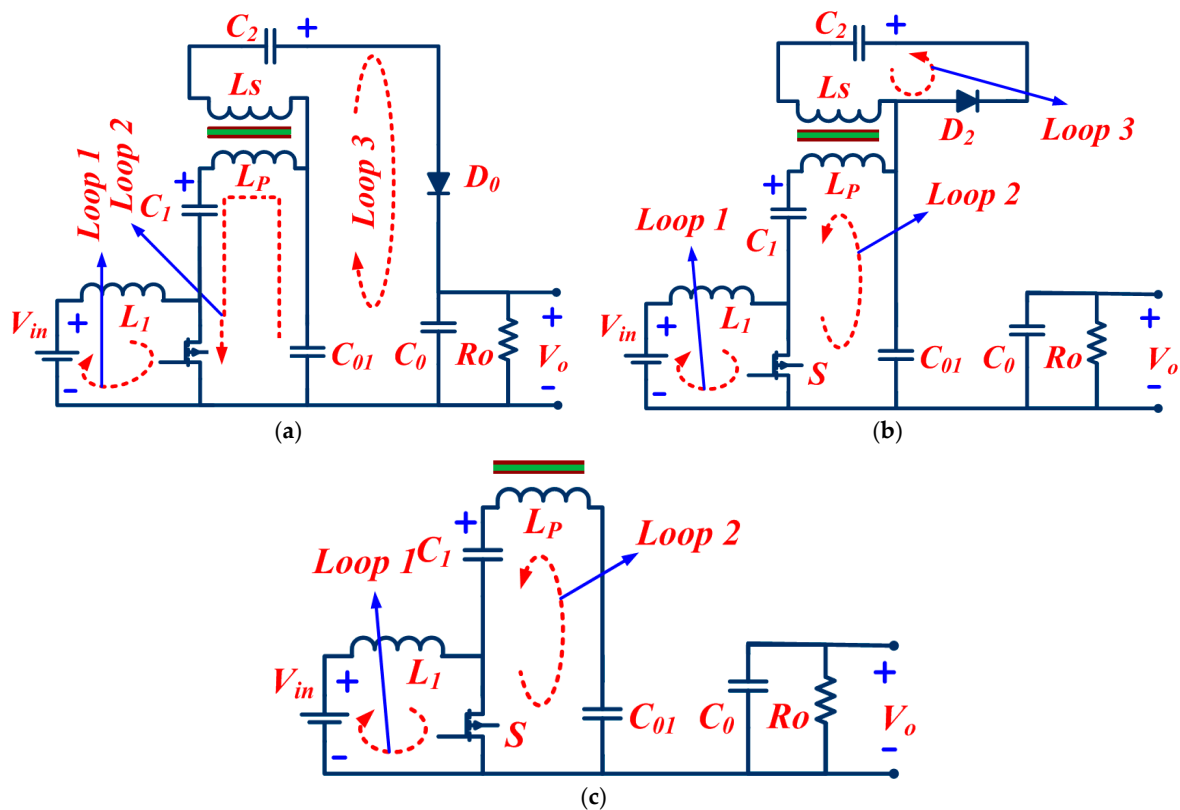

Figure 8. Equivalent circuit of proposed converter when switch S is in ON state (**a**) Mode-3 (Time *tc–td*); (**b**) Mode-4 (Time *td–te*); and (**c**) Mode-5 (Time *te–tf*).

2.4. Mode-4 (Time td–te)

In Mode-4, switch S is turned ON and inductor L_1 is continuously magnetized through switch S. The energy of the transformer windings Ls is transferred to capacitor C_2 through diode D_2. The energy conversion takes place in a resonant approach and the leakage inductance confines the current. The output capacitor C_0 provides energy to load. At the end of the mode capacitor C_2 is fully charged and diode D_2 is blocked. The equivalent circuit of proposed converter for this mode is shown in Figure 8b. In this mode diode D_2 are operated in forward biased condition whereas diode D_1, D_0 are operated in reverse biased.

$$\left. \begin{array}{c} Loop-1 \rightarrow V_{in} - V_{L1} = 0 \\ Loop-2 \rightarrow VC_1 - V_{LP} - VC_{01} = 0 \\ Loop-3 \rightarrow VC_2 = -V_{LS} \end{array} \right\} \tag{5}$$

2.5. Mode-5 (Time te–tf)

In Mode-5, switch S is turned ON and inductor L_1 is continuously magnetized through switch S. The energy of transformer windings Ls is not transferred to capacitor C_2 due to diode D_2 is in reverse biased. The output capacitor C_0 provides energy to load. The equivalent circuit of proposed converter for this mode is shown in Figure 8c. In this mode no diodes are operated in forward biased condition whereas diodes D_0, D_1, D_2 are in reverse biased condition.

$$\left. \begin{array}{c} Loop-1 \rightarrow V_{in} - V_{L1} = 0 \\ Loop-2 \rightarrow VC_1 = V_{LP} + VC_{01} \end{array} \right\} \tag{6}$$

The voltage conversion ratio (V_o/V_{in}) and Drain to Source voltage of switch (V_{DS}) of conventional boost converter with VD (power circuit of converter shown in Figure 5a) is calculated by Equation (7), where T is the total time of one switching cycle. The voltage conversion ratio (V_o/V_{in}) and (V_{DS}/V_{in}) of conventional boost converter with VD is shown graphically in Figure 9a. From graph it is observed that drain to source switch voltage is exactly half of the output voltage (for example at $D = 0.75$, $V_o/V_{in} = 8$ and $V_{DS}/V_{in} = 4$). Hence the drain to source voltage rating of the switch must be above four times of input to operate converter at 75% duty cycle.

$$\left. \begin{array}{c} \frac{V_o}{V_{in}} = \frac{2}{1-D} = \frac{2T}{T-t_{on}} \\ V_{DS} = \frac{1}{1-D} V_{in} = \frac{V_o}{2} = \frac{T}{T-t_{on}} V_{in} \end{array} \right\} \tag{7}$$
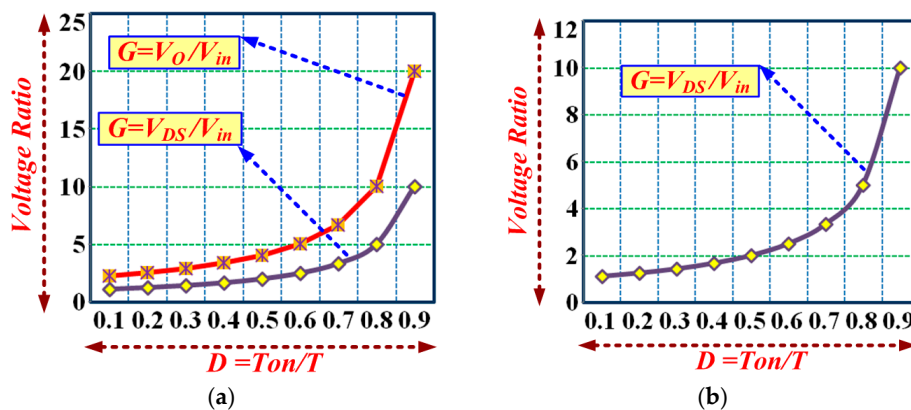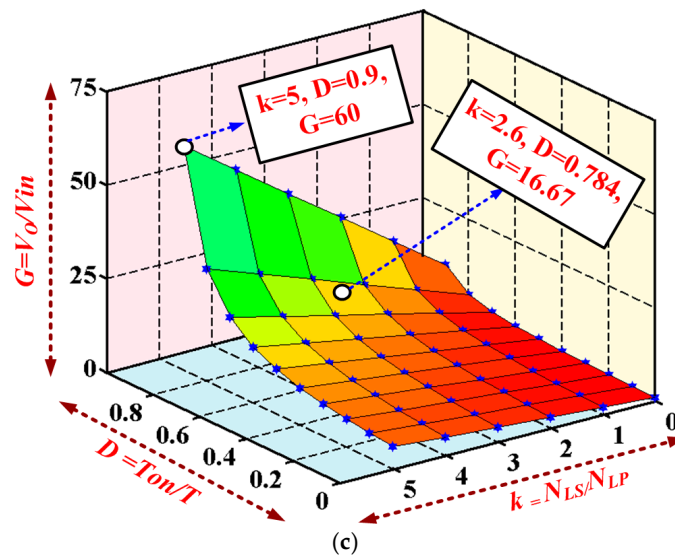

Figure 9. *Cont.*

(c)

Figure 9. Graphical plot (**a**) voltage conversion ratio (V_o/V_{in}) and Drain to Source switch voltage (V_{DS}) of conventional Boost converter with Voltage Doubler (V_D) versus duty cycle (D); (**b**) Drain to Source switch voltage (V_{DS}) of proposed T & SC-BC versus duty cycle (D); and (**c**) Relation between voltage conversion ratio (V_o/V_{in}), turns ratio, and duty cycle of proposed T & SC-BC.

The voltage conversion ratio (V_o/V_{in}) and Drain to Source voltage of switch (V_{DS}) of the proposed T & SC-BC are calculated by Equation (8), where T is the total time of one switching cycle. The relation of V_{DS}/V_{in} with duty cycle (D) is graphically shown in Figure 9b. The relation of voltage conversion ratio (V_o/V_{in}), turns ratio (k), and duty cycle (D) of the proposed T & SC-BC is shown graphically in Figure 9c. From the graphs it is observed that voltage conversion ratio is linearly increased with duty cycle and turns ratio. It is observed that the voltage conversion ratio is 16.67 at $D = 0.784$ when $k = 2.6$. The voltage conversion ratio is 60 at $D = 0.9$ when $k = 5$. It is also investigated that the drain to source switch voltage is exactly equal to the drain to source of a traditional boost converter with VD.

$$\left.\begin{array}{l} \dfrac{V_o}{V_{in}} = \dfrac{1+k}{1-D} = \dfrac{(1+k)T}{T-t_{on}} \\[2mm] V_{DS} = \dfrac{1}{1-D}V_{in} = \dfrac{V_o}{1+k} = \dfrac{T}{T-t_{on}}V_{in} \\[2mm] k = \dfrac{\text{Turns of Secondary winding of transformer } (N_{LS})}{\text{Turns of Primary winding of transformer } (N_{LP})} \end{array}\right\} \qquad (8)$$

3. Steady State Analysis of Transformer and Switch Capacitor Based Boost Converter (T & SC-BC)

In this section a steady state analysis of the proposed T & SC-BC is explained and the conversion losses, efficiency and voltage conversion ratio are calculated. In order to analyze the T & SC-BC, we consider the T & SC is working in steady state and the following assumptions are considered throughout the switching: (i) ripple free DC Source (V_{in}) (ii) diode D_1 semiconductor loss is V_{D1}; (iii) forward conduction loss of diode D_1 is modelled by ON-state resistance R_{D1} (efficiency of diode is 100% if V_{D1} and $R_{D1} = 0$); (iv) R_S is ON-state resistance of controlled switch. R_{L1} is internal resistance of winding of inductor L_1; (v) f_s is switching frequency (vi) ripple across capacitor is very small (vii) T & SC cell losses include copper loss, iron loss and diode conduction loss (viii) $R_{T\&SC}$ is the equivalent resistance of the T & SC cell. The steady state equivalent circuits of the T & SC-BC ON and OFF state are shown in Figure 10a,b respectively.

Consider i_{L1}, is and i_{c01} current is flowing through inductor L_1, switch S and capacitor C_{01} respectively. I_{L1}, Is and I_{C01} average current is flowing through inductor L_1, switch S and capacitor C_{01} respectively.
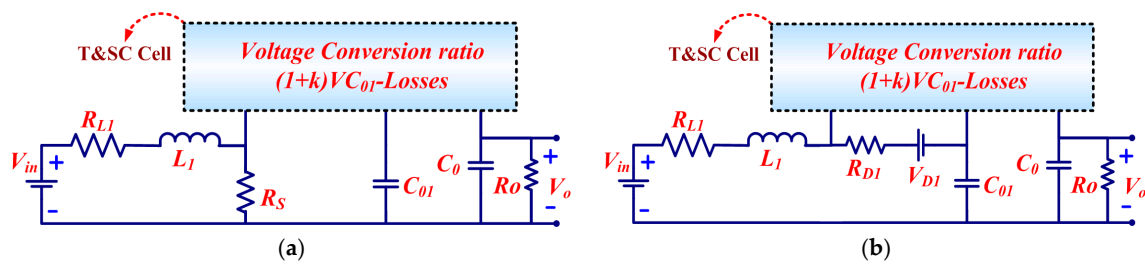
Figure 10. Equivalent circuit of T & SC-BC (**a**) ON state and (**b**) OFF state.

When switch is in ON state, diode D_1 is in reversed biased and inductor is charged by input supply V_{in}:

$$\left.\begin{array}{c} V_{in} - v_{L1} - i_{in}R_{L1} - i_s R_s = 0, i_{in} = i_s \\ v_{L1} = V_{in} - i_{in}(R_{L1} + R_s) \approx V_{in} - I_{in}(R_{L1} + R_s) \\ i_c(t) = -V_{c01}/R_{T\&SC} \end{array}\right\} \tag{9}$$

when switch is in OFF state, diode D_1 is conduct and inductor is discharged to charge capacitor C_{01}:

$$\left.\begin{array}{c} V_{in} - v_{L1} - i_{in}R_{L1} - i_{D1}R_{D1} - V_{D1} - V_{c01} = 0, i_{in} = i_{D1} \\ v_{L1} = V_{in} - i_{in}(R_{L1} + R_{D1}) - V_{D1} - V_{c01} \approx V_{in} - I_{in}(R_{L1} + R_{D1}) - V_{D1} - V_{c01} \\ i_c(t) = i_{in} - V_{c01}/R_{T\&SC} \end{array}\right\} \tag{10}$$

Inductor volt second balance method and capacitor charge method is used to calculate the voltage conversion ratio equation:

$$\left.\begin{array}{c} V_{c01} = \left(\frac{1}{1-D}\right)(V_{in} - (1-D)V_{D1})\left(\frac{(1-D)^2 R_{T\&SC}}{(1-D)^2 R_{T\&SC} + R_{L1} + DR_s + (1-D)R_{D1}}\right) \\ \frac{V_{c01}}{V_{in}} = \left(\frac{1}{1-D}\right)\left(1 - \frac{(1-D)V_{D1}}{V_{in}}\right)\left(\frac{1}{1 + \frac{R_{L1} + DR_s + (1-D)R_{D1}}{(1-D)^2 R_{T\&SC}}}\right) \end{array}\right\} \tag{11}$$

$$V_o = V_{c01}(1+k) - losses \text{ of transformer} \tag{12}$$

$$\left.\begin{array}{c} V_o = (1+k)\left(\frac{1}{1-D}\right)(V_{in} - (1-D)V_{D1})\left(\frac{(1-D)^2 R_{T\&SC}}{(1-D)^2 R_{T\&SC} + R_{L1} + DR_s + (1-D)R_{D1}}\right) \\ \frac{V_o}{V_{in}} = (1+k)\left(\frac{1}{1-D}\right)\left(1 - \frac{(1-D)V_{D1}}{V_{in}}\right)\left(\frac{1}{1 + \frac{R_{L1} + DR_s + (1-D)R_{D1}}{(1-D)^2 R_{T\&SC}}}\right) \end{array}\right\} \tag{13}$$

$$Conversion\ Losses = \left(\frac{1+k}{1-D}\right)\frac{(1-D)V_{D1}}{V_{in}}\left(\frac{1}{1 + \frac{R_{L1} + DR_s + (1-D)R_{D1}}{(1-D)^2 R_{T\&SC}}}\right) \tag{14}$$

$$\left.\eta, efficiency = \frac{\left(1 - \frac{(1-D)V_{D1}}{V_{in}}\right)}{1 + \frac{R_{L1} + DR_s + (1-D)R_{D1}}{(1-D)^2 R_{T\&SC}}}\right\} \tag{15}$$

If all the components efficiency is 100% (ideal components) then:

$$Losses = 0,\ \eta = 100\% \ and \frac{V_o}{V_{in}} = (1+k)\left(\frac{1}{1-D}\right) \tag{16}$$

The ideal voltage conversion ratio of T & SC-BC is given in Equation (16).

4. Comparison of Proposed Transformer and Switch Capacitor Based Boost Converter (T & SC-BC) with Newly Addressed DC-DC Converters

In this section the proposed T & SC-BC is compared with recently addressed DC-DC converters. Recently addressed converters are discussed in Section 1 of the article. In Table 1, the converter comparison is summarized in terms of voltage conversion ratio, number of inductors, number of switches, and number of diodes. First, it is observed that voltage conversion ratio of single switch

n-stage CBC is depends on the number of cascaded stages (*n*) and duty cycle. To design single switch *n*-stage CBC [30], *n*-number of inductors, *n*-number of capacitors and $2n - 1$ number of diodes along with single switch is required. Second, it is observed that voltage conversion ratio of single switch boost converter with voltage multiplier is depends on the odd and even number of voltage multiplier stage and duty cycle. To design single switch boost converter with voltage multiplier, 2 inductors, $2n + 1$ number of capacitors and $2n$ number of diodes along with single switch is required. Third, it is observed that voltage conversion ratio of coupled inductor based step-up converter is depends on the coupling coefficient of coupled inductor ($k = n_2/n_1$) and duty cycle. To design coupled inductor based step-up converter, 3 inductors (1 without coupling and 2 with coupled), 3 capacitors and 3 diodes along with single switch is required. Fourth, it is observed that voltage conversion ratio of Quadratic Boost Converter (QBC) with coupled inductor is depends on the coupling coefficient of coupled inductor ($k = n_2/n_1$) and duty cycle. To design Quadratic Boost Converter (QBC) with coupled inductor, 3 inductors (1 without coupling and 2 with coupled), 3 capacitors and 4 diodes along with single switch is required. Fifth, it is observed that to design conventional boost converter with VD 1 inductor, 3 capacitors, 1 switch and 3 diodes are required. Sixth, it is observed that voltage conversion ratio of proposed converter (T & SC-BC) is depends on the transformer turns ratio (*k*) and duty cycle. To design proposed converter (T & SC-BC), 1 inductor, 1 transformer, 4 capacitors and 3 diodes along with single switch is required.

Table 1. Comparison summary of the proposed T & SC-BC with recently addressed DC-DC converters.

DC-DC Converter	Voltage Conversion Ratio (V_o/V_{in})	Number of Switches	Number of Inductors	Number of Capacitors	Number of Diodes
Single switch *n*-stage CBC [38]	$\frac{1}{(1-D)^n}$	1	*n*	*n*	$2n - 1$
Single switch boost converter with voltage multiplier [38]	$\frac{n+D}{1-D}, n = 1,3\ldots$ $\frac{n+1+D}{1-D}, n = 2,4\ldots$	1	2	$2n + 1$	$2n$
Coupled inductor based step-up converter [39]	$\frac{1+(1+k)D}{1-D}, k = \frac{n_2}{n_1}$	1	3 (2 Inductor are Coupled)	3	3
Quadratic Boost Converter (QBC) with coupled inductor [40]	$\frac{1+kD}{(1-D)^2}, k = \frac{n_2}{n_1}$	1	3 (2 Inductor are Coupled)	3	4
Boost converter with voltage doubler (Figure 5a)	$\frac{2}{1-D}$	1	1	3	3
Proposed converter	$\frac{1+k}{1-D}, k = \frac{n_{LS}}{n_{LP}}$	1	1 Inductor with 1 transformer	4	3

n = Number of stages and *k* = Turns ratio.

Thus from Table 1 it is seen that the proposed converter required less components and has a higher voltage conversion ratio compared to the other discussed converters. In Table 2 the cost of the power circuit of the proposed T & SC-BC and recently addressed converters (discussed in Section 1) is tabulated and it is observed that the proposed converter requires less cost.

Table 2. Comparison of the proposed T & SC-BC with recent DC-DC converters in terms of cost.

DC-DC Converter	Cost of Converter
Single switch *n*-stage CBC [38]	$C_S + [n \times C_L] + [n \times C_C] + [(2n - 1) \times C_D]$
Single switch boost converter with voltage multiplier [38]	$C_S + [2 \times C_L] + [(2n + 1) \times C_C] + [(2n) \times C_D]$
Coupled inductor based step-up converter [39]	$C_S + [(1 \times C_{cL}) + (1 \times C_L)] + [3 \times C_C] + [3 \times C_D]$
QBC with coupled inductor [40]	$C_S + [(1 \times C_{cL}) + (1 \times C_L)] + [3 \times C_C] + [4 \times C_D]$
Boost converter with voltage doubler (Figure 5a)	$C_s + C_L + [3 \times C_C] + [3 \times C_D]$
Proposed T & SC-BC	$C_S + [(1 \times C_{cL}) + (1 \times C_T)] + [4 \times C_C] + [3 \times C_D]$

C_s = Cost of single switch, C_L = Cost of single inductor, C_C = Cost of single capacitor, C_D = Cost of single diode, C_T = Cost of Transformer, C_{CL} = Cost of two inductor with couple effect.

The plots of the voltage conversion ratio of a single switch CBC and single switch boost converter with voltage multiplier versus duty cycle considering the number of stages, *n* = 1 to 5 is depicted in

Figure 11a,b respectively. It is observed that the voltage conversion ratio increases with the increase in the number of cascaded stages, but the quasi-linear region of the converter decreases. The plot of the voltage conversion ratio of the coupled inductor based step-up converter and QBC with coupled inductor versus duty cycle considering coupling coefficients, $k = 1$ to 5 is depicted in Figure 11c,d respectively. It is observed that the voltage conversion ratio is greatly increased with the increase in coupling coefficient (k), but the quasi-linear region of the converter decreases.
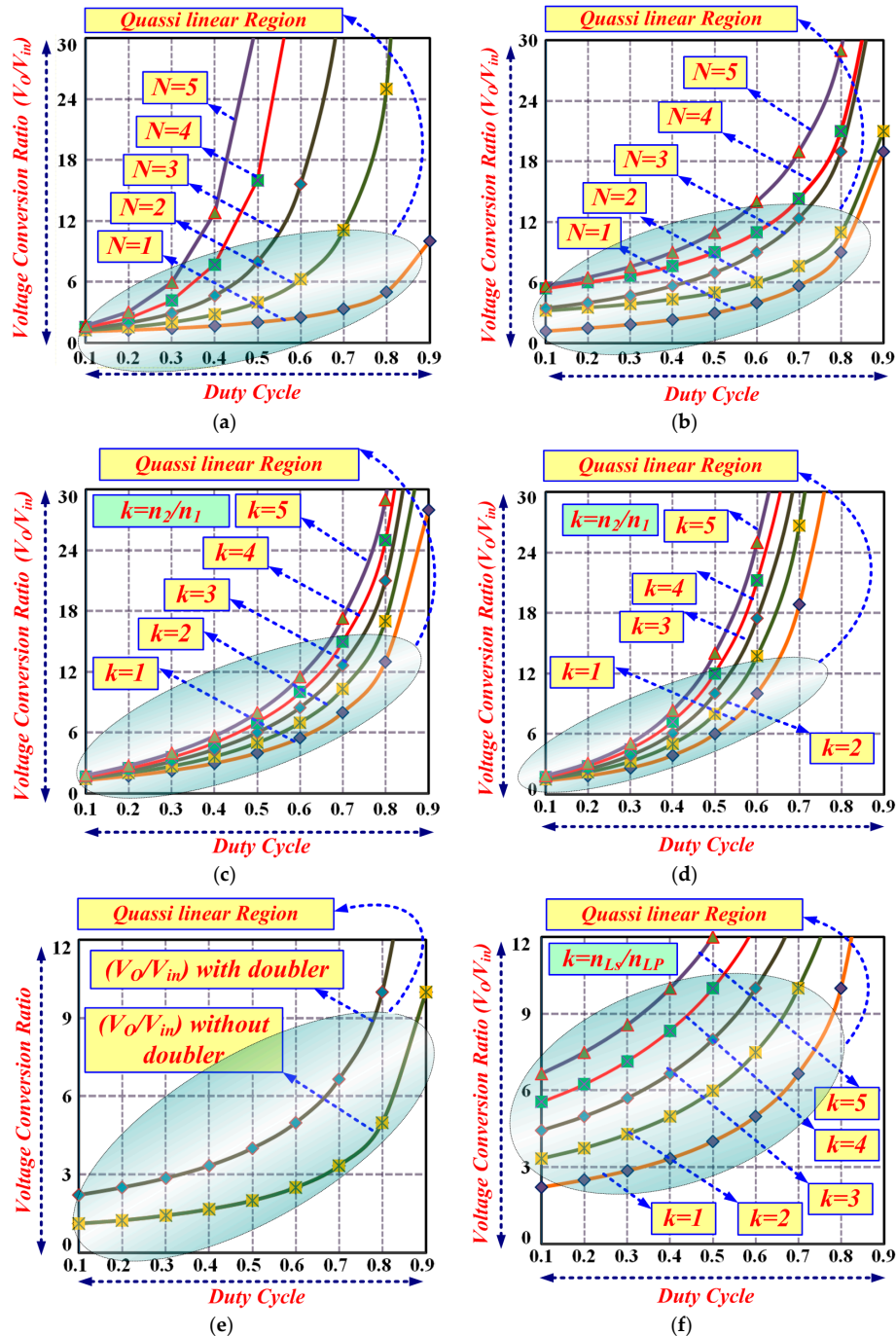
Figure 11. Plot of Voltage conversion ration versus Duty cycle (**a**) single switch *n*-stage CBC; (**b**) Single switch boost converter with voltage multiplier; (**c**) Coupled inductor based step-up converter; (**d**) Quadratic Boost Converter (QBC) with coupled inductor; (**e**) Conventional boost converter with Switched Capacitor (SC) or Voltage Doubler (VD) stage; and (**f**) Proposed Transformer and Switched Capacitor Based Converter (T & SC-BC).

The voltage conversion ratio and capacitor voltage plot of a conventional boost converter with or without SC or VD stage is depicted in Figure 11e. It is observed that the conversion ratio is double with the voltage doubler compared to without the voltage doubler but the quasi-linear region is slightly reduced. The voltage conversion ratio plot of the proposed T & SC-BC versus duty cycle considering transformer ratio, k = 1 to 5 is depicted in Figure 11f. It is observed that the voltage conversion ratio is greatly increased with the increase in number of the transformer ratio (k) but the quasi-linear region of the converter is decreased.

In Figure 12a, the plot of VC_n/V_{in} (ratio of capacitor voltage to input voltage) versus duty cycle for a single switch n-stage CBC is shown considering stages n = 1 to 5. It is observed that the capacitor rating increases with the increase in stages and duty cycle. Thus, a single switch n-stage CBC requires more rated capacitors compared to a single switch $n − 1$ stage CBC. In Figure 12b the plot of VC_{n1}/V_{in} and VC_{n2}/V_{in} (ratio of capacitor voltage to input voltage) versus duty cycle for a single switch boost converter with voltage multiplier is shown considering stage n = 1 to 5. It is observed that the rating of the capacitor increases with the increase in voltage multiplier stages and duty cycle. In Figure 12c the plot of VC_2/V_{in} (ratio of capacitor voltage to input voltage) versus duty cycle for a coupled inductor-based step-up converter is shown with coupling coefficients k = 1 to 5. It is observed that the capacitor voltage is independent of the coupling coefficient but depends upon the duty cycle.

In Figure 12d the plot of VC_{02}/VC_{01} (ratio of capacitor C_{02} voltage to capacitor C_{01} voltage) versus duty cycle for the QBC with coupled inductor is shown with coupled coefficients k = 1 to 5. It is observed that the capacitor voltage depends on the coupling coefficient and also on the duty cycle. Thus, the rating of the capacitor is increased with an increase in coupling coefficient (k) and duty cycle (D). In Figure 12e the plot of VC_{01}/V_{in} (ratio of capacitor C_{01} voltage to input voltage (V_{in})) versus duty cycle for the proposed T & SC-BC with transformer turn ratio k = 1 to 5. It is observed that the capacitor voltage is independent of the transformer ratio but depends upon the duty cycle. T & SC-BC is compared with recently addressed DC-DC converters (discussed in Section 1) in terms of the voltage conversion ratio (V_o/V_{in}) and the comparison plot is shown in Figure 12f. It is observed that the proposed T & SC-BC provides higher voltage conversion ratios compared to other DC-DC converters. T & SC-BC is compared with recently addressed DC-DC converters in term of V_{DS}/V_{in} (ratio of Drain to source voltage and input voltage) and the comparison plot is shown in Figure 12g and also tabulated in Table 3. It is observed that the proposed converter has a smaller V_{DS}/V_{in} ratio (ratio of Drain to Source voltage with respect input voltage), hence low rating components are suitable to design the T & SC-BC compared to recently proposed DC-DC converters (discussed in Section 1). Also in Table 3, T & SC-BC is compared in terms of efficiency; power range and output ripple with recent DC-DC converters.
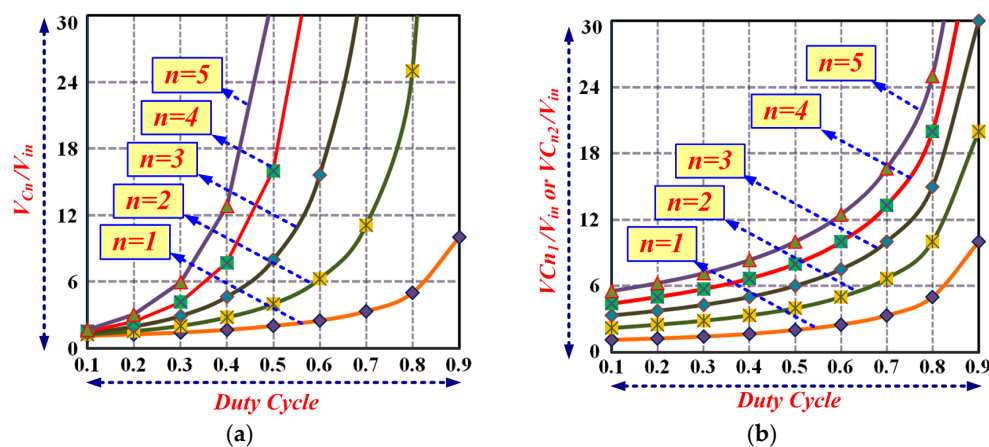

(a)　　　　　　　　　　　　　　　　　　　　(b)
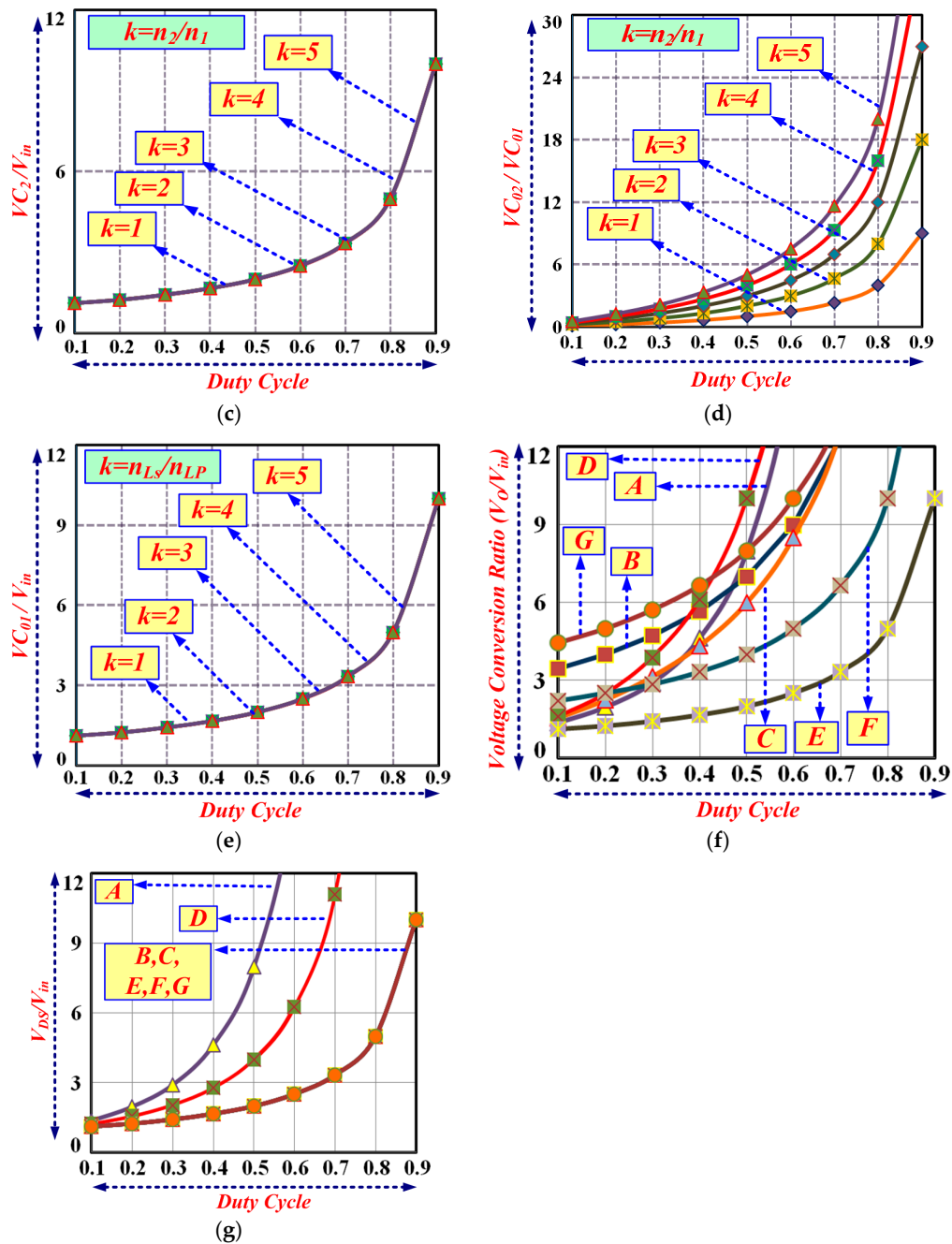
Figure 12. *Cont.*

(c)

(d)

(e)

(f)

(g)

Figure 12. (**a**) Plot of (VC_n/V_{in}) versus duty cycle for single switch *n*-stage CBC; (**b**) Plot of VC_{n1}/V_{in} and VC_{n2}/V_{in} versus duty cycle for single switch boost converter with voltage multiplier; (**c**) Plot of VC_2/V_{in} versus duty cycle for coupled inductor based step-up converter; (**d**) Plot of VC_{02}/VC_{01} versus duty cycle for QBC with coupled inductor; (**e**) Plot of VC_{01}/V_{in} versus duty cycle for proposed T & SC-BC; (**f**) Comparison of T & SC-BC and recently addressed DC-DC converter (discussed in Section 1) in terms of voltage conversion ratio (V_o/V_{in}); and (**g**) Comparison of T & SC-BC and recently addressed DC-DC converter (discussed in Section 1) in term of V_{DS}/V_{in} (ratio of Drain to source voltage and input voltage) with considering *n* = 3 and *k* = 3. (*A*: single switch *n*-stage CBC, *B*: single switch boost converter with voltage multiplier, *C*: coupled inductor based step-up converter, *D*: QBC with coupled inductor, *E*: Traditional Boost Converter, *F*: Traditional Boost Converter with Voltage Doubler (VD), *G*: Proposed T & SC-BC).

Table 3. Comparison of the proposed T & SC-BC with recently addressed DC-DC converters in terms of switch drain to source voltage.

DC-DC Converter	Switch Drain to Source Voltage (V_{DS})	Efficiency	Applications	Output Ripple
Single switch n-stage CBC [38] (Figure 2a)	$\frac{V_{in}}{(1-D)^n}, n = 1, 2, 3 \dots$	moderate (85–90%)	low/medium power	high
Single switch boost converter with voltage multiplier [38], (Figure 2b)	$\frac{V_{in}}{1-D}$	moderate (85–90%)	low/medium power	high
Coupled inductor based step-up converter [39], (Figure 2c)	$\frac{V_{in}}{1-D}$	high (90–95%)	medium/high power	low
Quadratic Boost Converter (QBC) with coupled inductor [40], (Figure 2d)	$\frac{V_O}{1+kD}, k = \frac{n_2}{n_1} = 1, 2, 3 \dots$	high (90–95%)	medium/high power	low
Conventional boost converter with voltage doubler (Figure 5a)	$\frac{V_{in}}{1-D}$	high (90–95%)	low/medium power	high
Proposed converter (Figure 5b)	$\frac{V_{in}}{1-D}$	high (90–95%)	medium/high power	low

5. Simulation and Experimental Results

To verify the proposed converter functionality, the proposed converter is simulated in Matrix Laboratory (MATLAB) and the parameters are tabulated in Table 4. The components are chosen and designed according to Equations (17)–(24).

$$Duty \ cycle, D = \frac{V_O - V_{in}(1+k)}{V_O} = \frac{250 - 15(1+2.6)}{250} = 0.784 \ or \ 78.4\% \tag{17}$$

$$Switch \ Voltage, V_{DS} = \frac{V_{in}}{1 - \frac{T_{ON}}{T}} = \frac{V_{in}}{1 - fT_{ON}} = \frac{V_{in}}{1 - D} = \frac{15}{1 - 0.784} = 69.44V \approx 70V \tag{18}$$

$$\left. \begin{array}{c} Diode \ D_0 \ Voltage, V_{D0} = \frac{n_{LS}}{n_{LP}} \times \frac{V_{in}}{1 - \frac{T_{ON}}{T}} \\ = \frac{kV_{in}}{1 - fT_{ON}} = \frac{kV_{in}}{1 - D} = \frac{2.6 \times 15}{1 - 0.784} = 180.5V \approx 181V \end{array} \right\} \tag{19}$$

$$Diode \ D_1 \ Voltage, V_{D1} = \frac{V_{in}}{1 - \frac{T_{ON}}{T}} = \frac{V_{in}}{1 - fT_{ON}} = \frac{V_{in}}{1 - D} = \frac{15}{1 - 0.784} = 69.44V \approx 70V \tag{20}$$

$$\left. \begin{array}{c} Diode \ D_2 \ Voltage, V_{D2} = \frac{n_{LS}}{n_{LP}} \times \frac{V_{in}}{1 - \frac{T_{ON}}{T}} \\ = \frac{kV_{in}}{1 - fT_{ON}} = \frac{kV_{in}}{1 - D} = \frac{2.6 \times 15}{1 - 0.784} = 180.5V \approx 181V \end{array} \right\} \tag{21}$$

$$Inductor, L_1 = \frac{V_{in} \times \frac{T_{ON}}{T}}{\Delta i L_1 \times f} = \frac{V_{in} \times DT}{\Delta i L_1} = \frac{15 \times 0.784}{5 \times 20000} = 117.6\mu H \tag{22}$$

$$Transformer \ Primary \ Winding, L_P = \frac{V_{in} \times \frac{T_{ON}}{T}}{\Delta i L_1 \times \frac{1}{T}} = \frac{V_{in} \times DT}{\Delta i L_1} = \frac{15 \times 0.784}{5 \times 20000} = 117.6\mu H \tag{23}$$

$$Transformer \ Secondary \ Winding, L_S = k^2 \times \frac{V_{in} \times \frac{T_{ON}}{T}}{\Delta i L_1 \times \frac{1}{T}} = k^2 \times \frac{V_{in} \times DT}{\Delta i L_1} = 794.97\mu H \tag{24}$$

The capacitors value of the proposed converter is calculated with the help of parameters voltage ripple through capacitors, switching frequency (f_s), current through capacitor and turn ratio of transformer (k). In Figure 13a the output voltage and input voltage waveform is depicted. It is observed that a constant 250 V is achieved with an input voltage of 15 V, hence the conversion ratio is 16.67.

The transient period analysis is investigated and it is observed that the time constant (τ) of output and input voltage waveforms is 0.006 s. The output and input voltage at 0.006 s is 157.5 V (63% of 250 V) and 9.45 V (63% of 15 V), respectively. It is observed that a constant 250 V is achieved at 0.035 s

(approximately). In Figure 13b the output voltage and current waveform are depicted. It is observed that the time constant (τ) of output voltage and current waveform is 0.006 s.

Table 4. Simulation parameters of the proposed T & SC-BC.

Parameter	Value
Input voltage (V_{in}), Output voltage (V_o)	15 V, 250 V
Input current (I_{in}), Output current (I_o)	3.34 A, 0.2 A
Power (P)	50 W
Duty cycle (D)	0.784
Switching frequency (f_s)	20 kHz
Switch Drain to Source voltage (V_{DS})	70 V (Minimum Voltage)
Inductor (L_1)	117.6 µH
Transformer windings	L_P = 117.6 µH, L_S = 794.97 µHTurns ratio, k = 2.6
Capacitors (C_1, C_2)	2.5 µF, 250 V
Capacitor C_0 and C_{01}	100 µF, 400 V

The output voltage and current at 0.006 s is 157.5 V and 0.126 A (63% of 0.2 A), respectively. It is observed that a constant 0.2 A is achieved at 0.035 s (approximately). In Figure 13c the output power waveform is depicted and it is observed that the output power at 0.006 s is 19.84 W. It is observed that a constant 50 W power is achieved at 0.035 s (approximately). In Figure 13d, the inductor (L_1) current waveform is depicted with gate pulse of the switch and slope of the waveforms is calculated by Equation (17). It is observed that the inductor (L_1) current slope is positive when switch S is in ON state and slope is negative when switch S is in OFF state. In Figure 13e, the switch drain to source voltage (V_{DS}) waveform is shown and nearly 70 V appears across the switch when it is in OFF state. A fluctuation is observed in the switch voltage due to the voltage across diode D_1 in the sub-modes. The voltage across capacitor C_1, C_2 and C_{01} is depicted in Figure 13f and it is observed that the voltage across capacitor C_{01} is 70 V (approximately). The voltage across diode D_0, D_1 and D_2 is depicted in Figure 13g and it is observed that diode D_0 is in forward biased when switch S is in OFF state. It is also that the voltage across D_1 is less than the voltage across diode D_0 and D_2. The proposed T & SC boost converter is implemented and the details of parameters or components are provided in Table 5. The experimental setup of the proposed converter is shown in Figure 14. The output voltage and input voltage waveforms are shown in Figure 15a,b. It is observed that 249.6 V is achieved from 15.1 V input supply.

$$\left.\begin{array}{l} \dfrac{di_{L1}}{dt} = \dfrac{VL_{1ON}}{L_1} = Positive\ Slope \\[2mm] \dfrac{di_{L1}}{dt} = \dfrac{VL_{1OFF}}{L_1} = Negative\ Slope \end{array}\right\} \tag{25}$$
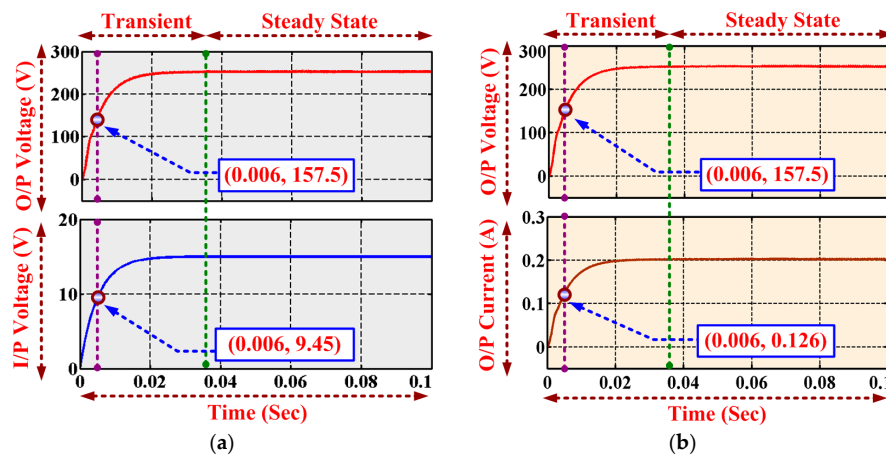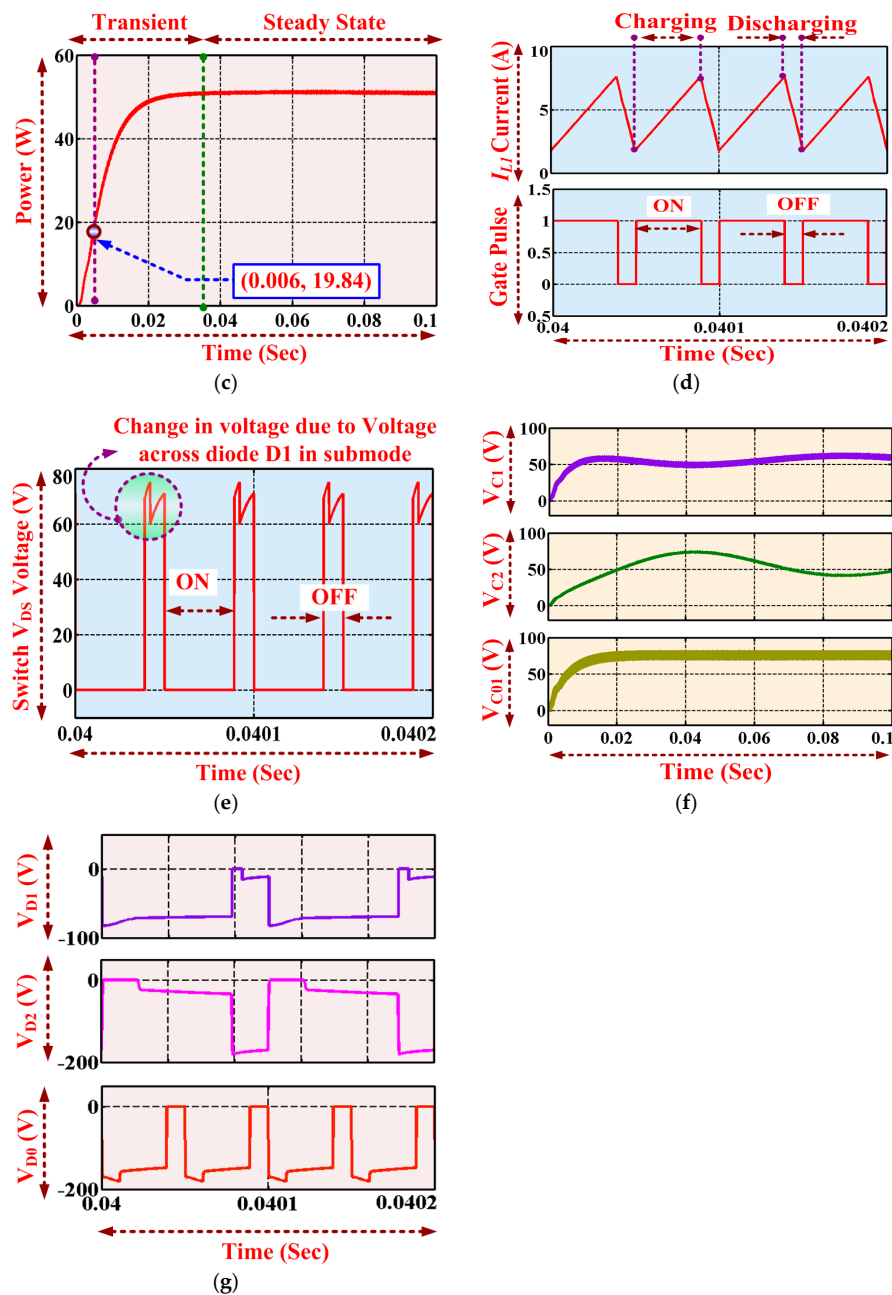

Figure 13. *Cont.*

Figure 13. Simulation result of the proposed T & SC-BC (**a**) Output and input voltage waveform; (**b**) Output voltage and current waveform; (**c**) Output power waveform; (**d**) Inductor L_1 current waveform and gate pulse (V_{GS}); (**e**) Drain to Source switch voltage (V_{DS}) waveform; (**f**) Voltage waveform across capacitor C_1, C_2 and C_{01}; and (**g**) Voltage waveform across diode D_0, D_1 and D_2.

Table 5. Parameters and component details of the prototype of the proposed T & SC-BC.

Parameter	Value
PV Panel	3 PV Panels (each of 18 V)
Input Voltage (V_{in}), Output Voltage (V_o)	15 V, 250 V
Input Current (I_{in}), Output Current (I_o)	3.34 A, 0.2 A
Power (P)	50 W
Duty Cycle (D)	0.784
Switching frequency (f_s)	20 kHz
Switch Drain to Source Voltage (V_{DS})	70 V (Minimum Voltage)
Inductor (L_1)	120 μH
Transformer Windings	L_P = 120 μH, L_S = 800 μH Turns ratio = 2.6
Capacitors (C_1 and C_2)	3.3 μF, 250 V
Capacitor C_0 and C_{01}	100 μF, 400 V
Diode (D_1, D_2, D_0)	MUR 860
Control Switch	IRF 540
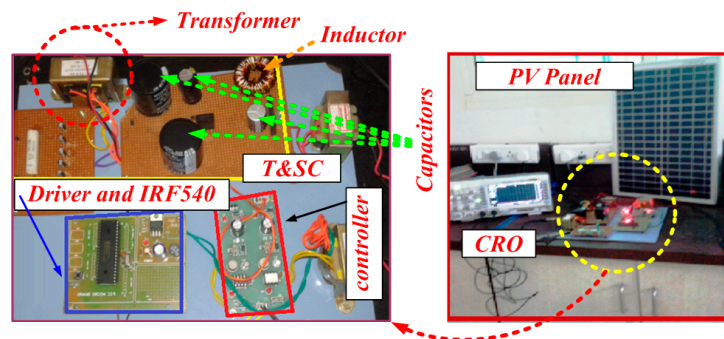
Figure 14. Experimental setup of the proposed T & SC Boost Converter.
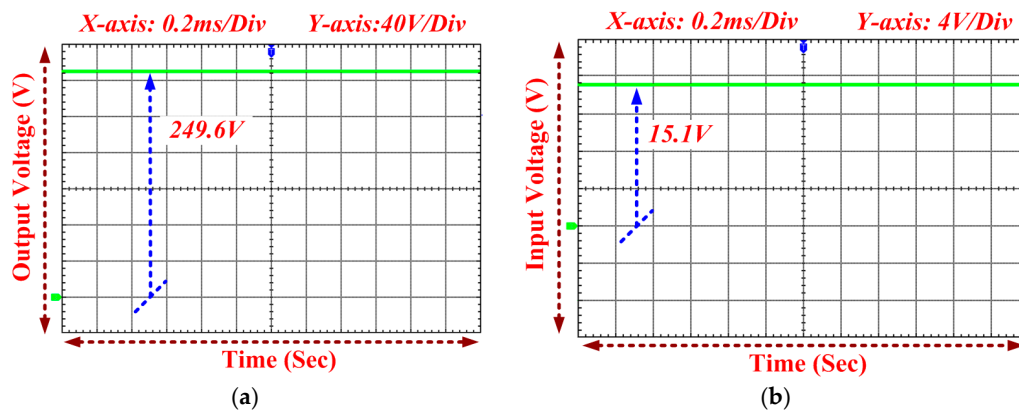
Figure 15. Experimental result (**a**) Output voltage waveform and (**b**) Input voltage waveform.

6. Future Extension and Combination of the Proposed T & SC-BC Topology with a Voltage Multiplier

To obtain a high voltage, the proposed T & SC-BC also provides a suitable solution by combining the features of a voltage multiplier. The power circuit of the proposed T & SC-BC with voltage multiplier is depicted in Figure 16. The voltage conversion ratio is analyzed and provided in Equation (26). The voltage across a switch is not affected by the voltage multiplier. The voltage

multiplier level can be increased without disturbing the main power circuit of the T & SC to raise the voltage conversion ratio more.

$$
\left.
\begin{array}{c}
\frac{V_{C01}}{V_{in}} = \frac{1+k}{1-D} = \frac{(1+k)T}{T-t_{on}}, \frac{V_{C03}}{V_{in}} = 2 \times \frac{1+k}{1-D} = 2 \times \frac{(1+k)T}{T-t_{on}} \\
\frac{V_{C05}}{V_{in}} = 3 \times \frac{1+k}{1-D} = 3 \times \frac{(1+k)T}{T-t_{on}}, \\
\frac{V_{C02N-1}}{V_{in}} = \frac{V_o}{V_{in}} = N\left(\frac{1+k}{1-D}\right) = N\frac{(1+k)T}{T-t_{on}} \\
V_{DS} = \frac{1}{1-D}V_{in} = \frac{V_{Co1}}{1+k} = \frac{V_o}{N(1+k)} = \frac{T}{T-t_{on}}V_{in} \\
k = \frac{Turns\ of\ Secondary\ winding\ of\ transformer\ (N_{LS})}{Turns\ of\ primary\ winding\ of\ transformer\ (N_{LP})} \\
N = number\ of\ voltage\ multiplier\ stage
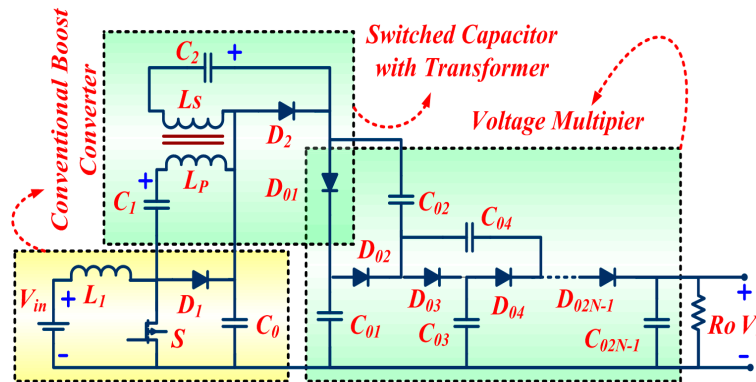\end{array}
\right\}
\tag{26}
$$

Figure 16. Power circuit of T & SC-BC with voltage multiplier (VM).

7. Conclusions

A new Transformer and Switch Capacitor-Based Boost Converter (T & SC-BC) is articulated for high-voltage/low-current renewable energy source applications. Conventional boost converter, transformer and switched capacitors functions are combined to design the proposed T & SC-BC for high voltage conversion ratio. A $(1+k)/(1-D)$ voltage conversion ratio (V_o/V_{in}) is achieved from the proposed converter where, k is the turns ratio of the transformer and D is the duty cycle. Conspicuous features of the proposed T & SC-BC are: (i) high voltage conversion ratio (V_o/V_{in}); (ii) continuous input current (I_{in}); (iii) single switch topology; (iv) single input source; (v) low Drain to Source voltage (V_{DS}) rating of the switch; and (vi) single inductor and single untapped transformer. The proposed T & SC-BC topology has low drain to source switch voltage, low stress on output diodes and requires less components to achieve high voltage compared to recently addressed DC-DC converters. Moreover the cost of the proposed T & SC-BC topology is less and it is also suitable for combination with a voltage multiplier to achieve more voltage at the output. The proposed converter is designed for 50/3 voltage conversion ratio at 78.4% duty cycle and the turns ratio is 2.6. Simulation and experimental results are provided which validate the functionality, design and concept of the proposed approach.

References

1. Hussain, S.; Al-ammari, R.; Iqbal, A.; Jafar, M.; Padmanaban, S. Optimization of Hybrid Renewable Energy System Using Iterative Filter Selection Approach. *IET Renew. Power Gener.* **2017**, *11*, 1440–1445. [CrossRef]
2. Chandramohan, K.; Padmanaban, S.; Kalyanasundaram, R.; Bhaskar, M.S.; Mihet-Popa, L. Grid Synchronization of Seven-phase Wind Electric Generator using d-q PLL. *Energies* **2017**, *10*, 926. [CrossRef]

3. REN21. Renewable 2017: Global Status Report. Available online: http://www.ren21.net/ (accessed on 14 June 2017).

4. REN21. Global Futures Report: Scenario Profiles Report. Available online: http://www.ren21.net (accessed on 16 January 2013).

5. Coster, E.J.; Myrzik, J.M.A.; Kruimer, B.; Kling, W.L. Integration issues of distributed generation in distribution grids. *Proc. IEEE* **2011**, *99*, 28–39. [CrossRef]

6. Teodorescu, R.; Liserre, M.; Rodriguez, P. *Grid Converters for Photovoltaic and Wind Power Systems*; Wiley: Hoboken, NJ, USA, 2011.

7. Padmanaban, S.; Pecht, M. An Isolated/Non-Isolated Novel Multilevel Inverter Configuration for Dual Three-Phase Symmetrical/Asymmetrical Converter. *Eng. Sci. Technol. Int. J.* **2016**, *19*, 1763–1770. [CrossRef]

8. Gunabalan, R.; Sanjeevikumar, P.; Blaabjerg, F.; Olorunfemi, O.; Subbiah, V. Analysis and Implementation of Parallel Connected Two Induction Motor Single Inverter Drive by Direct Vector Control for Industrial Application. *IEEE Trans. Power Electron.* **2015**, *30*, 6472–6475. [CrossRef]

9. Dragonas, F.A.; Nerrati, G.; Sanjeevikumar, P.; Grandi, G. High-Voltage High-Frequency Arbitrary Waveform Multilevel Generator for DBD Plasma Actuators. *IEEE Trans. Ind. Appl.* **2015**, *51*, 3334–3342. [CrossRef]

10. Türkay, B.; Telli, A.Y. Economic analysis of standalone and grid connected hybrid energy systems. *Renew. Energy* **2011**, *36*, 1931–1943. [CrossRef]

11. Energy Information Administration (EIA). International Energy Outlook 2009. United States Department of Energy; 2009. Available online: www.eia.doe.gov (accessed on 27 May 2009).

12. International Energy Agency (IEA). World Energy Outlook 2012. Available online: www.worldenergyoutlook.org (accessed on 12 November 2012).

13. Das, V.; Padmanaban, S.; Venkitusamy, K.; Selvamuthukumaran, R.; Blaabjerg, F.; Siano, P. Recent Advances and Challenges of Fuel Cell Based Power System Architectures and Control—A Review. *Renew. Sustain. Energy* **2017**, *73*, 10–18. [CrossRef]

14. Vavilapalli, S.; Sanjeevikumar, P.; Umashankar, S.; Mihet-Popa, L. Power Balancing Control for Grid Energy Storage System in PV Applications—Real Time Digital Simulation Implementation. *Energies* **2017**, *10*, 928. [CrossRef]

15. European Photovoltaic Industry Association (EPIA). *Global Market Outlook for Photo-Voltaic until 2013*; EPIA: Brussels, Belgium, 2009.

16. Timilsina, G.R.; Kurdgelashvili, L.; Narbel, P.A. Solar energy: Markets, economics and policies. *Renew. Sustain. Energy* **2012**, *16*, 449–465. [CrossRef]

17. Blaabjerg, F.; Yang, Y.; Ma, K.; Wang, X. Power Electronics—The key Technology for renewable energy system Integration. In Proceedings of the 4th International Conference on Renewable Energy Research and Application (ICRERA), Palermo, Italy, 22–25 November 2015.

18. Joshi, A.S.; Dincer, I.; Reddy, B.V. Performance analysis of photovoltaic systems: A review. *Renew. Sustain. Energy* **2009**, *13*, 1884–1897. [CrossRef]

19. Blaabjerg, F.; Ma, K.; Yang, Y. Power Electronics for Renewable Energy Systems—Status and Trends. In Proceedings of the 8th International Conference on Integrated Power Systems (CIPS), Nuremberg, Germany, 25–27 February 2014.

20. Liu, C.; Wu, B.; Cheung, R. Advanced Algorithm for Control of Photovoltaic Systems. In Proceedings of the Canadian Solar Buildings Conference, Montreal, QC, Canada, 20–24 August 2004.

21. Gupta, A.; Chauhan, Y.; Pachauri, R. A comparative investigation of maximum power point tracking methods for solar PV system. *Sol. Energy* **2016**, *136*, 236–253. [CrossRef]

22. Sanjeevikumar, P.; Grandi, G.; Wheeler, P.; Blaabjerg, F.; Loncarski, J. A Simple MPPT Algorithm for Novel PV Power Generation system by High Output Voltage DC-DC Boost Converter. In Proceedings of the 24th IEEE International Symposium on Industrial Electronics, Rio de Janeiro, Brazil, 3–5 June 2015; pp. 214–220.

23. Sanjeevikumar, P.; Blaabjerg, F.; Wheeler, P.; Ojo, J.O.; Ertas, A. High-Voltage DC-DC Converter Topology for PV Energy Utilization—Investigation and Implementation. *J. Electr. Power Compon. Syst.* **2016**, 1–12. [CrossRef]

24. Mahajan, S.B.; Sanjeevikumar, P.; Blaabjerg, F. A Multistage DC-DC Step-up Self Balanced and Magnetic Component–Free Converter for photovoltaic Application: Hardware Implementation. *Energies* **2017**, *10*, 719. [CrossRef]

25. Tofoli, F.L.; Pereira, D.C.; Paula, W.J. Comparative Study of Maximum Power Point Tracking Techniques for Photovoltaic Systems. *Int. J. Photoenergy* **2015**, *2015*, 812582. [CrossRef]

26. Jain, S.; Ramulu, C.; Padmanaban, S.; Ojo, J.O.; Ertas, A.H. Dual MPPT Algorithm for Dual PV Source Fed Open-End Winding Induction Motor Drive for Pumping Application. *Eng. Sci. Technol. Int. J.* **2016**, *19*, 1771–1780. [CrossRef]

27. Subudhi, B.; Pradhan, R. A comparative study on maximum power point tracking techniques for photovoltaic power systems. *IEEE Trans. Sustain. Energy* **2013**, *4*, 89–98. [CrossRef]

28. Gules, R.; dos Santos, W.M.; dos Reis, F.A.; Romaneli, E.F.R.; Badin, A.A. A Modified Sepic Converter with High Static gain for Renewable Applications. *IEEE Trans. Power Electron.* **2014**, *29*, 5860–5871. [CrossRef]

29. Meneses, D.; Blaabjerg, F.; Garcia, O.; Cobos, J. Review and comparison of step-up transformerless topologies for photovoltaic AC-Module application. *IEEE Trans. Power Electron.* **2013**, *28*, 2649–2663. [CrossRef]

30. Forouzesh, M.; Siwakoti, Y.; Gorji, S.; Blaabjerg, F.; Lehman, B. Step-up DC–DC Converters: A Comprehensive Review of Voltage Boosting Techniques, Topologies, and Applications. *IEEE Trans. Power Electron.* **2017**. [CrossRef]

31. Tofoli, F.L.; Dênis de Castro, P.; Josias de Paula, W.; de Sousa Oliveira Júnior, D. Survey on non-isolated high-voltage step-up dc–dc topologies based on the boost converter. *IET Power Electron.* **2015**. [CrossRef]

32. Prudente, M.; Pfitscher, L.; Emmendoerfer, G.; Romaneli, E.; Gules, R. Voltage multiplier cells applied to non-isolated DC–DC converters. *IEEE Trans. Power Electron.* **2008**, *23*, 871–887. [CrossRef]

33. Zhou, D.; Pietkiewicz, A.; Cuk, S. A Three-Switch high-voltage converter. *IEEE Trans. Power Electron.* **1999**, *14*, 177–183. [CrossRef]

34. Henn, G.; Silva, R.; Praca, P.; Barreto, L.; Oliveira, D. Interleaved boost converter with high voltage gain. *IEEE Trans. Power Electron.* **2010**, *25*, 2753–2761. [CrossRef]

35. Wai, R.; Lin, C.; Duan, R.; Chang, Y. High-Efficiency DC-DC converter with high voltage gain and reduced switch stress. *IEEE Trans. Ind. Electron.* **2007**, *54*, 1354–1364. [CrossRef]

36. Wai, R.; Duan, R. High-efficiency power conversion for low power fuel cell generation system. *IEEE Trans. Power Electron.* **2005**, *20*, 847–856. [CrossRef]

37. Li, W.; He, X. A family of interleaved DC–DC converters deduced from a basic cell with winding-cross-coupled inductors (WCCIs) for high step-up or step-down conversions. *IEEE Trans. Power Electron.* **2008**, *23*, 1791–1801. [CrossRef]

38. Young, C.; Chen, M.; Chang, T.; Ko, C.; Jen, K. Cascade Cockcroft–Walton Voltage Multiplier Applied to Transformer-less High Step-up DC–DC Converter. *IEEE Trans. Ind. Electron.* **2013**, *60*, 523–537. [CrossRef]

39. Tomaszuk, A.; krupa, A. High efficiency high step-up DC/DC converters—A review. *Bull. Pol. Acad. Sci. Tech. Sci.* **2011**, *59*. [CrossRef]

40. Chen, S.; Liang, T.; Yang, L.; Chen, J. A Cascaded High Step-up DC–DC Converter with Single Switch for Microsource Applications. *IEEE Trans. Power Electron.* **2011**, *26*. [CrossRef]

41. Mahajan, S.B.; Kulkarni, R.; Sanjeevikumar, P.; Siano, P.; Blaabjerg, F. Hybrid Non-Isolated and Non Inverting Nx Interleaved DC-DC Multilevel Boost Converter for Renewable Energy Applications. In Proceedings of the 16th IEEE International Conference on Environment and Electrical Engineering, Florence, Italy, 7–10 June 2016; pp. 1–6.

42. Mahajan, S.B.; Kulkarni, R.; Sanjeevikumar, P.; Blaabjerg, F.; Fedák, V.; Cernat, M. Non Isolated and Non-Inverting Cockcroft Walton Multiplier Based Hybrid 2Nx Interleaved Boost Converter for Renewable Energy Applications. In Proceedings of the 17th IEEE Conference on the Power Electronics and Motion Control, Varna, Bulgaria, 25–30 September 2016; pp. 146–151.

43. Mahajan, S.B.; Sanjeevikumar, P.; Blaabjerg, F.; Norum, L.; Ertas, A. 4Nx Non-Isolated and Non-Inverting Hybrid Interleaved Boost Converter Based on VLSI Cell and Cockroft Walton Voltage Multiplier for Renewable Energy Applications. In Proceedings of the IEEE International Conference on Power Electronics, Drives and Energy Systems, Trivandrum, India, 14–17 December 2016; pp. 1–6.

44. Mahajan, S.B.; Sanjeevikumar, P.; Ojo, O.; Marco, R.; Kulkarani, R. Non-Isolated and Inverting Nx Multilevel Boost Converter For Photovoltaic DC Link Applications. In Proceedings of the IEEE International Conference on Automatica, XXII Congress of the Chilean Association of Automatic Control, Talca, Chile, 19–21 October 2016; pp. 1–8.

45. Mahajan, S.B.; Sanjeevikumar, P.; Blaabjerg, F.; Kulkarni, R.; Seshagiri, S.; Hajizadeh, A. Novel LY Converter Topologies for High Gain Transfer Ratio-A New Breed of XY Family. In Proceedings of the 4th IET International Conference on Clean Energy and Technology (IET_CEAT16), Kuala Lumpur, Malaysia, 14–15 November 2016.

46. Mahajan, S.B.; Sanjeevikumar, P.; Wheeler, P.; Blaabjerg, F.; Rivera, M.; Kulkarni, R. XY Converter Family: A New Breed of Buck Boost Converter for High Step-up Renewable Energy Applications. In Proceedings of the Proceedings of the IEEE International Conference on Automatica, XXII Congress of the Chilean Association of Automatic Control (IEEE-ICA/ACCA'16), Talca, Chile, 19–21 October 2016; pp. 1–8.

47. Axelrod, B.; Berkovich, Y.; Ioinovici, A. Switched-Capacitor/Switched-Inductor structures for getting transformerless hybrid DC–DC PWM converters. *IEEE Trans. Circuits Syst. I Regul. Pap.* **2008**, *55*, 687–696. [CrossRef]

48. Villalva, M.; Gazoli, J.R.; Filho, E. Comprehensive Approach to Modeling and Simulation of Photovoltaic Arrays. *IEEE Trans. Power Electron.* **2009**, *24*, 1198–1208. [CrossRef]

49. Bendib, B.; Belmili, H.; Krim, F. A survey of the most used MPPT methods: Conventional and advanced algorithms applied for photovoltaic systems. *Renew. Sustain. Energy Rev.* **2015**, *45*, 637–648. [CrossRef]

50. Safari, A.; Mekhilef, S. Simulation and Hardware Implementation of Incremental Conductance MPPT with Direct Control Method Using Cuk Converter. *IEEE Trans. Ind. Electron.* **2011**, *58*. [CrossRef]

51. Saad Saoud, M.; Abbassi, H.; Kermiche, S.; Nada, D. Improved incremental conductance method for maximum power point tracking using cuk converter. *Mediterr. J. Model. Simul.* **2014**, *57–65*. Available online: http://www.webreview.dz/IMG/pdf/mjms_01_2014_057-065.pdf (accessed on 1 January 2014).

52. Hartmann, L.V.; Vitorino, M.A.; de Rossiter Correa, M.B.; Lima, A.M.N. Combining model-based and heuristic techniques for fast tracking the maximum power point of photovoltaic systems. *IEEE Trans. Power Electron.* **2013**, *28*, 2875–2885. [CrossRef]

53. Esram, T.; Chapman, P. Comparison of Photovoltaic Array Maximum Power Point Tracking Techniques. *IEEE Trans. Energy Convers.* **2007**, *22*. [CrossRef]